MacLaren, I. and Richter, G. (2009) *The structure and possible origins of stacking faults in gamma-yttrium disilicate.* Philosophical Magazine, 89 (2). pp. 169-181. ISSN 1478-6443

http://eprints.gla.ac.uk/4894/

Deposited on: 26 January 2009

The structure and possible origins of stacking faults in gamma-yttrium disilicate

I. MacLaren[a*] and G. Richter[b]

[a]*Department of Physics and Astronomy, Faculty of Physical Sciences, University of Glasgow, Glasgow G12 8QQ, UK;* [b]*Max-Planck-Institut für Metallforschung, Heisenbergstr. 3, D-70569 Stuttgart, Germany*

Parallel stacking faults on (010) planes are frequently observed in hot-pressed $Y_2Si_2O_7$. A combination of conventional dark-field imaging and high-resolution transmission electron microscopy was used to investigate the structure of these faults and it was found that they consist of the repeat of one layer of the two layer γ-$Y_2Si_2O_7$ structure with an associated in-plane rigid body displacement. The resulting structure was confirmed by image simulation of high-resolution images from two perpendicular projections. A model for the formation of the stacking faults is proposed as a consequence of a transformation from β-$Y_2Si_2O_7$ to γ-$Y_2Si_2O_7$ in the hot pressing.

Keywords: Yttrium silicates; stacking faults, TEM; image simulation

---

[*] Corresponding author, email: ian.maclaren@physics.org
Formerly at *Institut für Materialwissenschaft, TU-Darmstadt, Petersenstr. 23, D-64287 Darmstadt, Germany* and *Max-Planck-Institut für Metallforschung, Heisenbergstr. 5, D-70569 Stuttgart, Germany* where large portions of the work reported in this paper were carried out

1. Introduction

Yttrium silicates have excellent high temperature mechanical properties and display these until very close to their melting points. They are also fully oxidised and do not contain volatile components and thus are suitable for use in highly oxidising environments. For this reason, they have been investigated as possible matrix materials for oxide-oxide ceramic matrix composites [1,2] and as oxidation barrier coatings for non-oxide ceramic matrix composites [3-6].

Yttrium disilicate, along with the rare-earth disilicates, displays a remarkable polymorphism and this is well reviewed by Liddell and Thompson [7] and by Felsche [8]. Four well-characterised phases: α (triclinic), β (monoclinic), γ (monoclinic), and δ (orthorhombic) are known to exist. Furthermore, another less well characterised phase, normally denoted y, is also known [7,9], and often occurs in Y-doped SiAlONs [10,11]. Lastly, two different forms of δ were distinguished by Dinger *et al*. [12] using high-resolution TEM. The four well-characterised phases have been shown to be in the relation:

$$\alpha \xleftrightarrow{1225°C} \beta \xleftrightarrow{1445°C} \gamma \xleftrightarrow{1535°C} \delta \qquad (1)$$
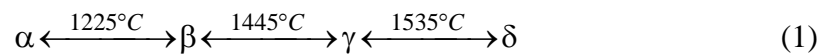
by Ito and Johnson [13]. These temperatures are however affected by preparation techniques and may vary somewhat [10]. Moreover, impurities or doping elements may affect the phase equilibria since in Si_3N_4 and SiAlONs, the main observed phases are normally y, β and δ [11,12,14] and other phases such as α and γ are not seen.

One major problem, however, with yttrium disilicate is that the yttria and silica react very slowly with one another and it is therefore difficult to achieve phase equilibrium, especially when prepared by mixed oxide methods. Thus, the precursor powder for the ceramic studied in this work was prepared by a chemical synthesis

route [1], to ensure atomic scale mixing of the SiO_2 and Y_2O_3 complexes prior to calcination and sintering. In view of the difficulty in sintering such materials, as for instance typified in the work of Aparicio *et al.* [4] hot pressing was used to produce $Y_2Si_2O_7$ ceramics. This study then concentrates on the structure and origins of the frequently observed planar faults in the resulting material, using transmission electron microscopy as the primary experimental tool.

2. Materials preparation and experimental procedure

Amorphous yttrium disilicate precursor powders were prepared from yttrium acetate and tetraethylorthosilicate as described previously [1,2]. These were then mixed with 3 wt. % LiF and then hot pressed at 10 MPa and 1600 °C resulting in the formation of a dark-coloured plate with a density of 3.48 g cm^{-3} corresponding to 86 % of the theoretical density of γ-$Y_2Si_2O_7$.

The material was prepared for transmission electron microscopy (TEM) using a standard procedure of cutting, grinding and polishing from both sides, doubled-sided dimpling, and argon ion milling (Gatan PIPS, 5 kV, ± 4°), followed by carbon coating to prevent charging. Conventional diffraction contrast TEM observations were performed with a JEOL 2000FX and a Philips CM20, both operated at 200 kV (both Stuttgart). High-resolution TEM (HRTEM) was performed with a JEOL 4000EX operated at 400 kV (MPI-Stuttgart), the Stuttgart ARM operated at 1250 kV and a JEOL 3010 equipped with a Gatan Image Filter (GIF) operated at 297 kV (TU-Darmstadt).

Approximate defocus values for HRTEM images were determined at the microscope using the deviation from the minimum contrast condition and from analysis of the contrast at amorphous regions at the specimen edges using the NCEM

Focus Determination Package [15] for the Gatan Digital Micrograph software package. These and other parameters were then refined using the Iterative Digital Image Matching method [16] where the cross-correlation between experimental and simulated images of perfect crystal is maximised by iteratively varying the various electron optical parameters. Once the parameters had been optimised, experimental defect images were compared with those simulated from a model defect structure, and atoms were then allowed to relax using a similar iterative procedure to maximise the cross-correlation, thus making possible the determination of the atomic structure of defects.

3. Structural details of the yttrium disilicates

As stated above the four well-characterised phase of $Y_2Si_2O_7$. These are briefly summarised in Table 1 below. The structural parameters are taken from Liddell and Thompson [7], with the exception of those for γ-$Y_2Si_2O_7$, which are taken from a more recent study of Leonyuk *et al*. [17]. The information on bonding was derived from the earlier review article of Felsche [8]. Since the majority of this paper concerns the γ-$Y_2Si_2O_7$ phase, two important projections of this crystal structure,[100] and [001], are shown in Figure 1. This shows two layers of Si_2O_7 double tetrahedra along the length of the long b-axis alternating in a zigzag fashion.

Structure	α-$Y_2Si_2O_7$	β-$Y_2Si_2O_7$	γ-$Y_2Si_2O_7$	δ-$Y_2Si_2O_7$
Symmetry	Triclinic	Monoclinic	Monoclinic	Orthorhombic
Space group	$P\bar{1}$	C2/m	$P2_1/c$	$Pna2_1$

a	6.59 Å	6.875 Å	4.694 Å	13.66 Å
b	6.64 Å	8.970 Å	10.856 Å	5.020Å
c	12.25 Å	4.721 Å	5.588 Å	8.152 Å
α	94.0°	90°	90°	90°
β	89.2°	101.74°	96°	90°
γ	93.1°	90°	90°	90°
Si-O bonding	Si_3O_{10} triple corner sharing tetrahedra and SiO_4 single tetrahedra	Si_2O_7 double corner sharing tetrahedra	Si_2O_7 double corner sharing tetrahedra	Si_2O_7 double corner sharing tetrahedra

Table 1: Crystal structure details for the main crystalline $Y_2Si_2O_7$ polymorphs

4. Results and analysis

4.1. Long parallel faults

As reported previously [18], the microstructure of the hot-pressed compact consists of grains having the γ-$Y_2Si_2O_7$ structure, containing approximately spherical glassy inclusions and crossed by numerous planar faults, all of which lie predominantly on the same crystallographic plane. The grains have a composition close to the stoichiometric $Y_2Si_2O_7$ composition, with perhaps a slight tendency to small Si excesses, and the glassy inclusions are primarily SiO_2 with about 2.5 cat % Y present. This microstructure is shown in Figure 2, which shows clearly the frequent

parallel planar faults as fine lines. In every case examined, the grains displayed the γ-$Y_2Si_2O_7$ structure as for instance illustrated by the indexed diffraction pattern of Figure 3.

Figure 4 shows dark field TEM images of a stacking fault in an yttrium disilicate grain. In Figure 4a taken using the $20\bar{2}$ diffraction vector, the fault is clearly visible and inclined to the beam direction. The majority of the fault lies on one crystallographic plane, although two steps on other planes can be seen (A and B). The fault terminates at a partial dislocation (D). A silica-glass inclusion is also visible (G). When the fault is imaged with the 040 diffraction vector as shown in Figure 4b it is edge-on, out-of-contrast and lies perpendicular to the diffraction vector. The partial dislocation is, however, still in contrast, and some residual contrast is shown at step A, suggesting a different local relaxation at the fault on this plane. Other studies confirm this and show that the faults lie primarily on the (010) planes and that **g.R** is integer or near-integer for **g** = 040.

In order to understand why the faults arise on the (010) planes it is necessary to revisit the crystal structure. As may be seen in Figure 1, the structure of gamma yttrium disilicate consists of a zigzag structure of Si_2O_7 double tetrahedra along the b-axis. Perpendicular to this, there are gaps every half unit cell. Thus, it would be easy to remove one of the sets of double tetrahedra resulting in the repeat of the same orientation of double tetrahedra. In this case, no significant disruption would be caused to the double tetrahedra and all that would be required would be a suitable rigid body displacement at the fault in order to maintain good bonding and minimise electrostatic repulsion across the fault.

To determine the details of the stacking fault structure, it is most convenient to use high-resolution transmission electron microscopy to image the stacking faults edge-on

at atomic resolution. Figure 5a shows an HRTEM image of a stacking fault taken along the [100] zone axis of the crystal. The unit cells are shown in outline along with the zigzag structure of the layers. It is clear to see that a layer is repeated at the fault core, as expected. The rigid body displacement at the interface in the plane perpendicular to [100] could also be measured by measuring the displacement of the unit cells on the one side of the fault with respect to those on the other side. Figure 5b shows an HRTEM image of the same boundary taken along the almost perpendicular [001] zone axis. Again a zigzag structure is shown and again the rigid body displacement in this plane could be measured. Combining these two measurements of the rigid body displacement the fault displacement vector, **R**, was determined to be [0.26, 0.48, -0.73]. This diffraction vector would also give **g.R** ≈ integer for **g** = 040, thus giving the contrast extinction in diffraction contrast noted in Fig 4b. Thus, the diffraction contrast TEM and HRTEM results are in good agreement. Using this **R** vector a model structure for the fault could be constructed and this is shown in Figure 6, once again using the two projections [100] and [001].

In order to test this stacking fault structure, image simulations were performed for each of the images of Figs 5a and 5b. Firstly, the image simulation was compared with the experimental image for an area of perfect crystal near the fault and the electron optical parameters iteratively changed to optimise the cross-correlation. The resulting parameters are shown in Table 2.

	Fig 5a – [100] projection	Fig 5b – [001] projection
Microscope	JEOL 4000EX (Stuttgart)	JEOL 3010 (Darmstadt)
Sample thickness	9.1 nm	11.4 nm
Defocus	-72 nm	-52 nm

2-fold astigmatism	7.5 nm @ 10.3°	4.3 nm @ 104°
3-fold astigmatism	71 nm @ 6.5°	249 nm @ 32°
Coma	0.3 nm @ 0.8°	299.6 nm @ 118.4°

Table 2: Iteratively determined electron optical parameters for the images of Figures 5a and 5b.

The tabulated parameters were then used in the simulation of the fault images. In both cases 10 unit cells along the fault were averaged from the experimental images to provide a better signal to noise ratio for the comparison. The experimental and simulated images were then compared with one another and in both cases showed extremely high cross-correlation coefficients, demonstrating that the model structure and displacement vector, **R**, are extremely good. Some attempts were made to change **R** slightly but these always resulted in reduced cross-correlation coefficient. The Y and Si atoms close to the fault were then allowed to relax in the simulation until the cross-correlation was maximised resulting in cross-correlations of 94.3 % and 92 % for the images of Figures 5a and 5b, respectively. The experimental, simulated and difference images are then shown in Figures 7a and 7b, respectively. A colour representation was used to enhance the otherwise very low contrast difference images. These show the extremely good match between the simulated structures and the experimental images and demonstrate that we can have confidence in the measured **R** vector and associated model structure of Figure 6.

4.2. Steps on the stacking faults

The steps A and B in Figure 3a were also studied by stereographic trace analysis to determine their habit planes. Figure 8 shows a picture of another arrangement of steps on some stacking faults and their habit planes were also determined in the same manner. The results are summarised in Table 3 below. It should be noted that the steps are generally rather short and this leads to large errors in orientation determination by trace analysis. Thus errors in the determination of the habit plane of 5-10° would not be surprising.

Step	Habit plane	Angular Deviation	From low-index plane
A	(0.99, -0.21, -0.03)	5.3°	(100)
B	(0.03, 1.83, -0.73)	6.9°	$(02\overline{1})$
C	(-0.91, -0.97, 0.09)	4.5°	$(\overline{1}\,\overline{1}0)$

Despite the large errors in the determination of the habit planes, it is very clear that each step has a distinctly different habit and no clear pattern seems to emerge. It can only be concluded that there are several possible habit planes for steps and that there is no obvious low energy choice for a step if the stacking fault has to deviate from the (010) plane. Now if we examine the diagrams of the γ-$Y_2Si_2O_7$ structure shown in Figure 1 it is plain that there is little opportunity to shift the structure or remove layers of any planes perpendicular to the [100] direction without cutting through the double tetrahedra or introducing corrugations. The $(02\overline{1})$ plane can be represented in this projection and it would necessarily be rather corrugated to avoid cutting the double tetrahedra. This is shown in Figure 9. It is perhaps more

straightforward to imagine shifts or missing planes on the (100) plane by looking at the [001] projection, and this is also indicated on Figure 9. Similarly, the $(\bar{1}\,\bar{1}0)$ plane seems to cut between the double tetrahedra and seems also to represent a way of shifting the plane off (010) without causing too much structural disruption.

Whatever the precise structure of the steps, it is clear that they are relatively high energy in comparison to the (010) plane stacking faults, since they account for only a small proportion of the stacking fault surface area. The relatively high energy is not surprising in view of the amount of structural disruption caused by losing planes and introducing shifts on any plane other than (010) since this may disrupt the double tetrahedra, or place or tetrahedra at energetically unfavourable distances from one another.

Stacking faults are occasionally observed to end within grains, rather than at grain boundaries, and this always occurs at partial dislocations as seen in Fig 3a, as is crystallographically necessary. The density of either partial or lattice dislocations is uniformly low in all samples observed, and this suggests that there was no significant plastic deformation of the grains by slip during hot pressing. Thus, the partial dislocations are unlikely to be the result of slip processes. Rather they seem to have arisen from the same process that formed the stacking faults, as discussed below.

4.3. Possible formation mechanism for the stacking faults

It was previously observed that the precursor powder behaved much as in earlier reports of the crystallisation of pure yttrium disilicate [13] in that it crystallised to the α, β and γ phases at successively higher temperatures [1]. Furthermore, previous work has shown that the crystallisation of the amorphous precursor to α-$Y_2Si_2O_7$ occurs very rapidly on heating in just a narrow temperature window, and that

this is a highly exothermic reaction [2]. Thus, we can be sure that the ceramic was initially transformed to α-$Y_2Si_2O_7$ and it is highly likely that this transformed to β-$Y_2Si_2O_7$ prior to the formation of γ-$Y_2Si_2O_7$.

Now the α-$Y_2Si_2O_7$ and β-$Y_2Si_2O_7$ structures are totally different in that α-$Y_2Si_2O_7$ consists of Si_3O_{10} triple tetrahedra and SiO_4 single tetrahedra whereas the β-$Y_2Si_2O_7$ just contains Si_2O_7 corner sharing double tetrahedra. Thus, any transformation from α-$Y_2Si_2O_7$ to β-$Y_2Si_2O_7$ is completely reconstructive involving bond-breaking and new bond formation. Consequently no crystallographic correspondence is expected between the two phases, and we expect few microstructural relics of this the transformation. A similar argument would also apply if the α-$Y_2Si_2O_7$ transformed directly to γ-$Y_2Si_2O_7$ since this, like β-$Y_2Si_2O_7$ contains only Si_2O_7 corner sharing double tetrahedra. Thus, no microstructural relics such as stacking faults would be expected from transformations from α-$Y_2Si_2O_7$ to β-$Y_2Si_2O_7$ or even α-$Y_2Si_2O_7$ direct to γ-$Y_2Si_2O_7$ without first passing through the β-$Y_2Si_2O_7$ phase.

Now in some systems, a structure can order from a higher symmetry to a lower symmetry such as in an ordering transition or in a ferroelastic phase transition. Crystallographically, the ordered phase has a low symmetry space group, which is a sub-group of the space group of the original higher symmetry phase. Now if the transformation starts at two different places in a grain with different orientational or translational states related by a symmetry operator of the higher symmetry parent phase (which is suppressed in the lower symmetry phase) then some form of domain boundary must form. A general crystallographic discussion of this effect is given by Van Tendeloo and Amelinckx [19]. The present transformation does not, however, fulfil this above criterion; the γ-$Y_2Si_2O_7$ phase has a *higher* symmetry (space group

number 14, $P2_1/c$) than the parent β-$Y_2Si_2O_7$ phase (space group number 12, $C2/m$) and there is no simple subgroup-supergroup relationship.

Nevertheless, there are definite correspondences between the two phases in that both consist of corner sharing Si_2O_7 double tetrahedra with Y atoms between. Therefore one could be transformed to the other by shuffles of the Y atoms and movement and/or rotation of the double tetrahedra. One model that could lead to this is shown in Figure 10 where $[010]_\gamma//[010]_\beta$ and $[100]_\gamma//[100]_\beta$. The double tetrahedra would have to be rotated from the beta phase orientation to the gamma phase orientation, but the sense of rotation adopted in different parts of the prior beta crystal could be opposite. Thus, we would end up with two gamma crystals that differ just by being half a unit cell out of phase. This could be represented by one region with the double tetrahedra in a zig-zag-zig-zag order, and another having the double tetrahedra in a zag-zig-zag-zig order. Thus, inevitably at the boundary there will be two zigs or two zags adjacent to one another, resulting in the formation of a stacking fault.

Whilst a model has been presented for how the frequent stacking faults could arise, and it does seem likely that they are a relic of the β-$Y_2Si_2O_7$ to γ-$Y_2Si_2O_7$ transformation, it is not yet possible to confirm this hypothesis. To do so would require the production of samples at just the right sintering temperature so that the two phases coexist. Then it would be possible to determine the orientation relationship between the two and if stacking faults are really arising as a consequence of the transformation.

5. Conclusions

Parallel stacking faults on (010) planes are a common feature of γ-$Y_2Si_2O_7$. High resolution transmission electron microscopy was used along different projections in

the (010) plane to determine the structure of the faults and the displacement vector could be readily determined from the unit cell displacement across the fault in two perpendicular projections along [100] and [001]. The structure of γ-$Y_2Si_2O_7$ is a two layer structure and the fault was found to correspond to the repeat of one layer, with an associated rigid body shift in the plane of the boundary. Image simulations of the fault corresponded very well with the experimental images, thus confirming the structure model.

Occasional deviations from the (010) plane are also noted for the stacking faults and the resulting steps were analysed and found to lie on various planes. No single preferred step plane could be found and it was concluded that all steps are energetically unfavourable and only adopted where necessity forces the fault plane away from (010). Stacking faults were also occasionally observed to end at partial dislocations, but their density was very low and there was little evidence for any dislocation slip at any time in the preparation of the sample.

A possible formation mechanism for the faults was proposed, as a consequence of the β-$Y_2Si_2O_7$ to γ-$Y_2Si_2O_7$ transformation during hot-pressing, but further experiments would be needed to confirm both the transformation mechanism and the fault formation mechanism.

specification transmission electron microscopes) by Prof. Manfred Rühle and Prof

Hartmut Fuess. IM is indebted to the Alexander von Humboldt foundation for

provision of a research fellowship at the MPI in Stuttgart.

References

[1] P.A. Trusty, K.C. Chan, and C.B. Ponton, J. Mater. Res. 13 (1998) p.3135.

[2] I. MacLaren, P.A. Trusty, and C.B. Ponton, Acta Mater. 47 (1999) p.779.

[3] J.D. Webster, M.E. Westwood, F.H. Hayes et al., J. Eur. Ceram. Soc. 18 (1998) p.2345.

[4] M. Aparicio, R. Moreno, and A. Duran, J. Eur. Ceram. Soc. 19 (1999) p.1717.

[5] M. Aparicio and A. Duran, J. Am. Ceram. Soc. 83 (2000) p.1351.

[6] M. Aparicio and A. Duran, Ceram. Int. 31 (2005) p.631.

[7] K. Liddell and D.P. Thompson, Brit. Ceram. Trans. J. 85 (1986) p.17.

[8] J. Felsche, Struct. Bond. 13 (1973) p.99.

[9] N.G. Batalieva and Yu.A. Pyatenko, Sov. Phys. Crystallography 16 (1972) p.786.

[10] J. Parmentier, P.R. Bodart, L. Audoin et al., J. Sol. Stat. Chem. 149 (2000) p.16.

[11] I. MacLaren, L.K.L. Falk, A. Díaz et al., J. Eur. Ceram. Soc. 21 (2001). p.2937

[12] T.R. Dinger, R.S. Rai, and G. Thomas, J. Am. Ceram. Soc. 71 (1988) p.236.

[13] J. Ito and H. Johnson, Am. Mineral. 53 (1968) p.1940.

[14] W.E. Lee, C.H. Drummond, G.E. Hilmas et al., J. Am. Ceram. Soc. 73 (1990) p.3575.

[15] R. Kilaas, NCEM Focus Determination Package . Available online at: http://ncem.lbl.gov/frames/software.htm (accessed July 2005).

[16] G. Möbus and M. Rühle, Ultramicroscopy, 56 (1994) 54.

[17] N.I. Leonyuk, E.L. Belokoneva, G. Bocelli et al., Cryst. Res. Technol. 34 (1999) p.1175.

[18] I. MacLaren, R. Schierholz, P. A. Trusty et al., J. Am. Ceram. Soc. 90 (2007) p.3307.

[19] G. Van Tendeloo and S. Amelinckx, Acta Cryst. A30 (1974) p.431.

Figure Captions

Figure 1: Representations of the γ-$Y_2Si_2O_7$ crystal structure for the [100] and [001] projections. The Si_2O_7 double tetrahedra are clearly seen. The isolated atoms between the tetrahedra are the Y atoms.

Figure 2: Bright field TEM image of the structure of a typical yttrium disilicate grain showing stacking faults (SF) and glassy inclusions (G).

Figure 3: [100] zone axis selected area diffraction pattern of γ-$Y_2Si_2O_7$.

Figure 4: Dark field images of the same stacking fault, SF, recorded with two different diffraction conditions, a grain boundary, GB, and a glassy inclusion, G, are also shown: a) was recorded with $\mathbf{g} = 20\bar{2}$ and shows all parts of the fault in strong contrast; b) was recorded with $\mathbf{g} = 040$ and shows the main part of the fault and the step B out of contrast, but step A still shows some weak contrast. C is a partial dislocation at the end of the fault

Figure 5: HRTEM images of the structure of stacking faults recorded using different projections with unit cells and dot pairs (which approximately correspond to Y atom positions) indicated. The repeated layer at the stacking fault is clear in both images: a) [100] recorded on the JEOL 4000EX at Stuttgart; b) [001] recorded on the JEOL 3010 at Darmstadt

Figure 6: Models of the stacking fault structure for the [100] and [001] projections.

Figure 7: Image matching for the HRTEM images along a) the [100] and b) the [001] projections. From left to right, average of 10 atomic cells of the experimental image, best simulated image, difference plot. The stacking fault plane is indicated by a dotted line in each image.

Figure 8: Dark field TEM image of steps on stacking faults in γ-$Y_2Si_2O_7$.

Figure 9: Schematic diagram of how different step planes could fit through the unit cell.

Figure 10: Schematic diagram of how the beta to gamma transformation could proceed.
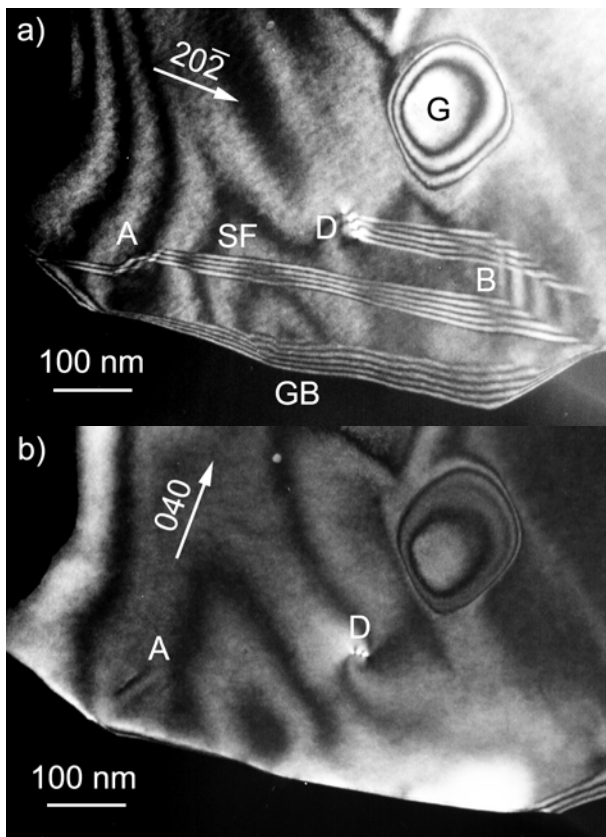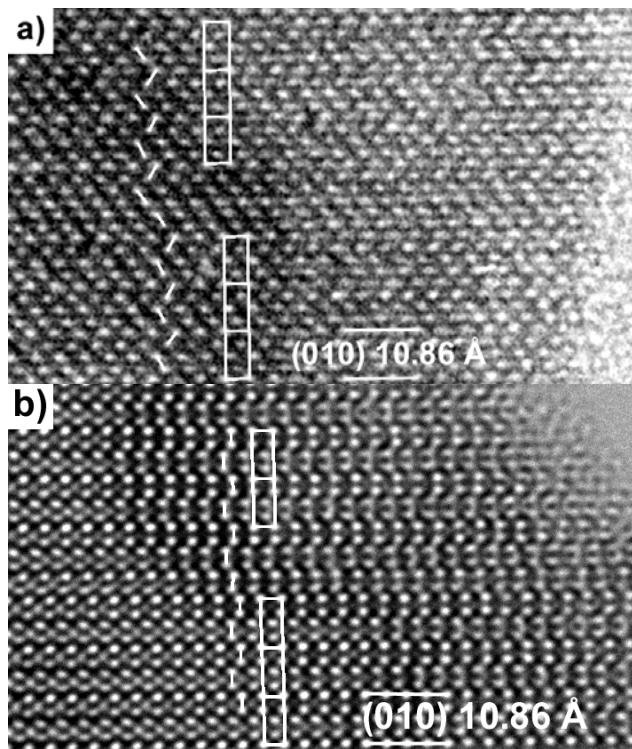
Figure 1:

[100]   [001]
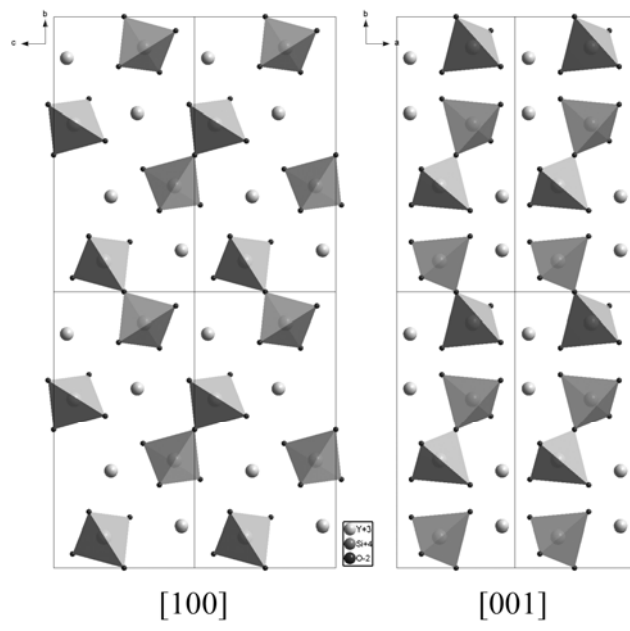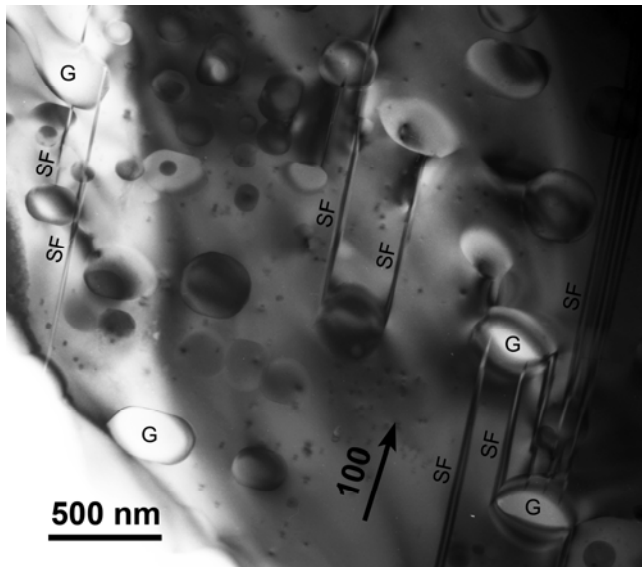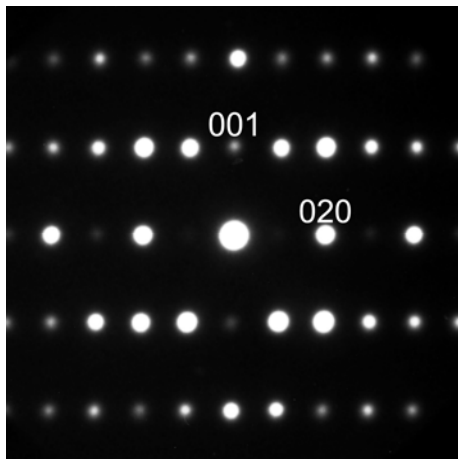
Figure 2
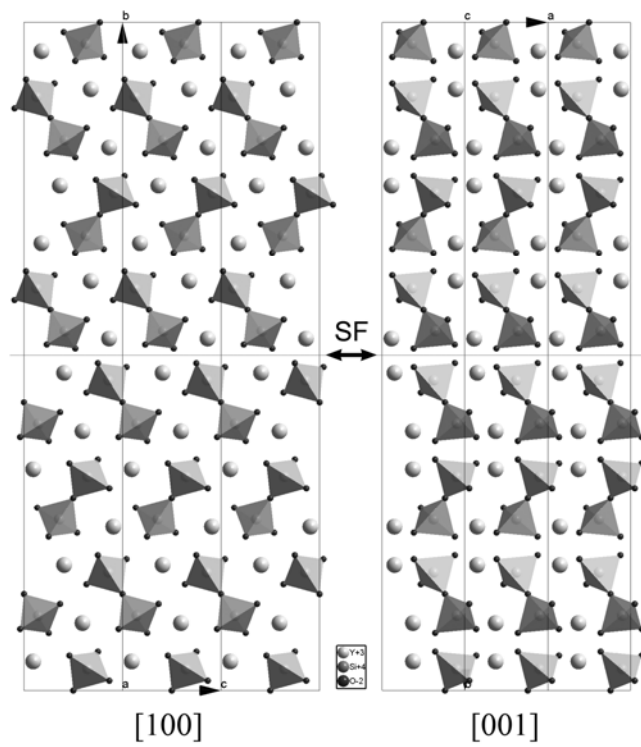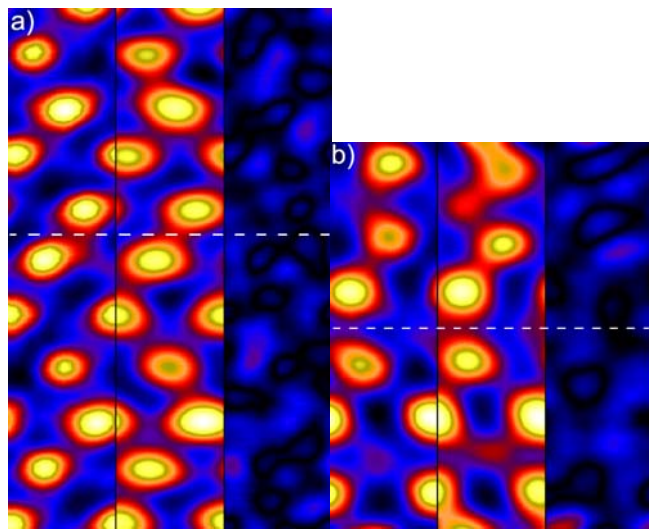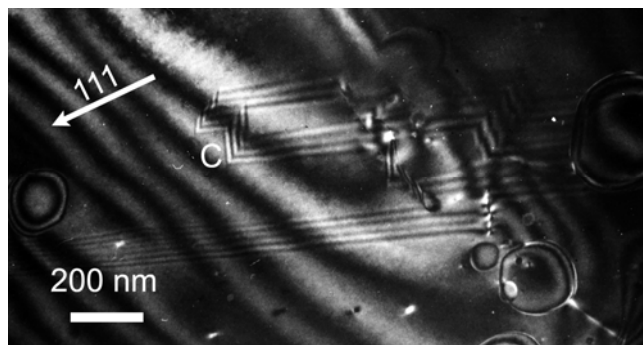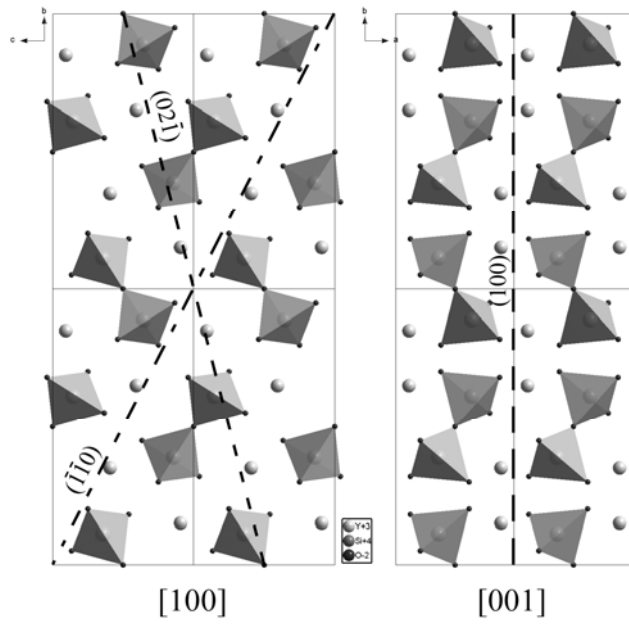
Figure 3

Figure 4

Figure 5

Figure 6

Figure 7

Figure 8

Figure 9

[100]   [001]

Figure 10

β-Y$_2$Si$_2$O$_7$ [001]   γ-Y$_2$Si$_2$O$_7$ [001]